

Cathepsin C promotes colorectal cancer metastasis by regulating immune escape through upregulating CSF1

Yun-Zhi DANG^{1,2,*}, Xiao-Jiao CHEN³, Jiao YU¹, Shu-Hong ZHAO¹, Xi-Ming CAO¹, Qing WANG¹

¹Department of Radiation Oncology, Shaanxi Provincial People's Hospital, Xi'an, China; ²State Key Laboratory of Cancer Biology, Fourth Military Medical University, Xi'an, China; ³Xi'an Medical University, Xi'an, China

*Correspondence: dangyunzhi@xjtu.edu.cn

Received July 26, 2022 / Accepted January 23, 2023

Since metastasis remains the primary reason for colorectal cancer (CRC) associated death, a better understanding of the molecular mechanism underlying CRC metastasis is urgently needed. Here, we elucidated the role of Cathepsin C (CTSC) in promoting CRC metastasis. The expression of CTSC was detected by real-time PCR and immunohistochemistry in the human CRC cohort. The metastatic capacities of CTSC-mediated metastasis were analyzed by *in vivo* metastasis model. Elevated CTSC expression was positively associated with tumor differentiation, tumor invasion, lymph node metastasis, and AJCC stage and indicated poor prognosis in human CRC. CTSC overexpression in CRC cells promoted myeloid-derived suppressor cells (MDSCs) and tumor-associated macrophages (TAMs) recruitment by the CSF1/CSF1R axis. In contrast, the knockdown of CSF1 reduced CTSC-mediated MDSCs and TAMs infiltration and CRC metastasis. Depletion of either MDSCs or TAMs decreased CTSC-mediated CRC metastasis. In human CRC tissues, CTSC expression was positively associated with intratumoral MDSCs and TAMs infiltration. Furthermore, the combination of CTSC inhibitor AZD7986 and anti-PD-L1 antibody blocked CTSC-induced CRC metastasis. CTSC overexpression promoted MDSCs and TAMs infiltration by CSF1/CSF1R axis. Interruption of this oncogenic loop may provide a promising treatment strategy for inhibiting CTSC-driven CRC metastasis.

Key words: colony stimulating factor 1; myeloid-derived suppressor cell; tumor-associated macrophage; AZD7986

Colorectal cancer (CRC) is one of the most common causes of cancer-related deaths worldwide [1]. The vast majority of CRC-related deaths result from metastasis to distant organs, such as the liver and lung [2]. Although systemic treatment has made great progress, the 5-year survival rate is still very low in patients with metastatic CRC. In recent years, targeted therapy and immunotherapy have shifted the treatment paradigm for CRC. However, because of the low response rate, treatment of CRC remains challenging in clinical practice [2]. Recent studies exhibited encouraging results on advanced CRC with combined therapy [3], which implies that combination therapy may provide a potential treatment option for some CRC subpopulations.

Cathepsin C (CTSC), also known as dipeptidyl peptidase I, is a cysteine protease found in lysosomes. Many serine proteases, including proteinase 3 (PR3), neutrophil elastase (NE), cathepsin G (CTSG), granzyme A/B/C, and mast cell chymase, require it for catalytic activation [4–5]. CTSC controls immunological responses and signaling pathways in normal cells. CTSC dysfunction is linked to many inflamma-

tory disorders, including Wegener granulomatosis, rheumatoid arthritis, pneumonia, and viral infection [6]. In addition, abnormal CTSC activity can promote neutrophil serine protease inactivation, which can cause Papillon-Lefevre syndrome [7] or Haim-Monk syndrome [8]. Upregulation of CTSC expression can affect the tumor microenvironment by influencing the process of numerous growth regulators such as chemokines and cytokines [9]. CTSC has been shown to function as an oncogene and lead to malignant behaviors in kinds of human cancer, including squamous, pancreatic, and breast cancer [10, 11]. Khaket et al. found that CTSC promoted CRC cell proliferation by regulating autophagy [12]. In addition, CTSC targeting plays a key role in regulating autophagy-mediated CRC cell proliferation [13]. These studies indicated that CTSC may play a role in CRC progression. However, whether CTSC is involved in CRC metastasis remains unclear.

Immunoediting is a dynamic process of immunosurveillance to immune escape, which can lead tumors to be poorly immunogenic [14]. The tumor microenvironment,

https://doi.org/10.4149/neo_2023_220726N757

Cathepsin C promotes colorectal cancer metastasis by regulating immune escape through upregulating CSF1

Yun-Zhi DANG^{1,2*}, Xiao-Jiao CHEN³, Jiao YU¹, Shu-Hong ZHAO¹, Xi-Ming CAO¹, Qing WANG¹

Supplementary Information

Supplementary Table S1. Chemokines and receptors RT² profiler PCR array of SW480-control vs. SW480-CTSC.

Gene	Description	Fold change	Gene	Description	Fold change
CSF1	colony stimulating factor 1	5.12	CXCL5	chemokine (C-X-C motif) ligand 5	1.84
CXCL5	chemokine (C-X-C motif) ligand 5	3.71	CXCL16	chemokine (C-X-C motif) ligand 16	1.82
CXCL3	chemokine (C-X-C motif) ligand 3	3.62	BMP7	Bone morphogenetic protein 7	1.80
CXCL1	chemokine (C-X-C motif) ligand 1	3.49	CXCL2	chemokine (C-X-C motif) ligand 2	1.75
ACKR2	Atypical Chemokine Receptors 2	3.45	CCL17	Chemokine (C-C motif) ligand 17	1.56
CCR2	chemokine (C-C motif) receptor 2	3.44	CCL20	Chemokine (C-C motif) ligand 20	1.43
CSF1R	colony stimulating factor 1 receptor	3.21	GPI	Glucose-6-phosphate isomerase	1.41
IL6	Interleukins 6	3.10	FASLG	Fas ligand	1.35
CCL3	Chemokine (C-C motif) ligand 3	3.05	IL4	Interleukin 4	1.24
ACKR4	Atypical Chemokine Receptors	3.01	CCL2	Chemokine (C-C motif) ligand 2	1.15
CCL20	chemokine (C-C motif) ligand 20	2.91	IL3	Interleukin 3	1.04
CXCL10	chemokine (C-X-C motif) ligand 10	2.85	GPI	Glucose-6-phosphate isomerase	1.01
CXCL2	chemokine (C-X-C motif) ligand 2	2.75	CCL22	Chemokine (C-C motif) ligand 22	-1.05
CCL20	Chemokines 20	2.66	OSM	Oncostatin M	-1.11
CCL5	Chemokine (C-C motif) ligand 5	2.71	IL12B	Interleukin 12B	-1.22
IL8	Interleukin 8	2.71	IL7	Interleukin 7	-1.28
ADH6	alcohol dehydrogenase 6	2.60	TNF	Tumor necrosis factor	-1.31
SLC7A11	solute carrier family 7-member 11	2.60	OSM	Oncostatin M	-1.35
AKR1B10	aldo-keto reductase family 1, member B10 (aldose reductase)	2.67	CD40LG	CD40 ligand	-1.42
CXCL3	chemokine (C-X-C motif) ligand 3	2.67	CCL22	Chemokine (C-C motif) ligand 22	-1.49
IL1B	Interleukin-1B	2.45	CCL24	Chemokine (C-C motif) ligand 24	-1.57
CXCR1	α -Chemokine (CXC Motif)1	2.33	IL18	Interleukin 18	-1.63
CCL7	Chemokine (C-C motif) ligand 7	2.21	MIF	Macrophage migration inhibitory factor	-1.68
IL10	Interleukin10	2.19	IL27	Interleukin 27	-1.74
SPP1	Secreted phosphoprotein 1	2.16	BMP7	Bone morphogenetic protein 7	-1.78
LTB	Lymphotoxin beta (TNF superfamily, member 3)	2.14	IL1RN	Interleukin 1 receptor antagonist	-1.82
IL17A	Interleukin 17A	2.07	IL1A	Interleukin 1, alpha	-1.93
CXCL11	chemokine (C-X-C motif) ligand 11	2.04	TNFRSF11	Tumor necrosis factor receptor superfamily, member 11	-2.01
CCL4	Chemokine (C-C motif) ligand 4	1.95	TNFRSF10	Tumor necrosis factor (ligand) superfamily, member 10	-2.22
CCL20	Chemokine (C-C motif) ligand 20	1.93	CCL7	Chemokine (C-C motif) ligand 7	-2.43
CCL8	Chemokine (C-C motif) ligand 8	1.90	CCL21	Chemokine (C-C motif) ligand 24	-2.52
IL10	Interleukin 10	1.89			

composed of various cellular and non-cellular factors, plays a pivotal role in cancer metastasis [15]. Among the multiple factors which can lead to the loss of immunogenicity, the recruitment of suppressive immune cells is one dominant driver [16]. Intratumoral MDSCs and TAMs infiltration correlated with a poor prognosis in human CRC [17]. MDSCs and TAMs suppress CD8⁺ T cell function by depriving amino acids via arginase-I expression, releasing oxidizing molecules, and stimulating other immunosuppressive cells. However, the haptic oncogenic signal in CRC that stimulates MDSCs and TAMs recruitment and activation is still poorly understood.

Here, we demonstrated that CTSC was upregulated and associated with a poor prognosis in CRC. Overexpression of CTSC promoted CRC metastasis by upregulating CSF1. The administration of CTSC inhibitor AZD7986 and anti-PD-L1 markedly suppressed CTSC-mediated CRC metastasis.

Materials and methods

Cell lines. All human cell lines were purchased from the American Type Culture Collection (ATCC), Manassas, VA, USA. Murine colon cancer cell line, MC38 was purchased from OBiO Technology (Shanghai) Co., Ltd. MC38 cells were cultured in Dulbecco's Modified Eagle Medium (DMEM) medium supplemented with 10% FBS, 100 µg/ml penicillin, and 100 µg/ml streptomycin. The cell lines SW620 and SW480 were cultured in RPMI-1640 medium with 10% FBS, 100 µg/ml penicillin, and 100 µg/ml streptomycin.

Construction of lentivirus and stable cell lines. Lentiviral vectors encoding shRNAs were generated using pLKO.1-TRC (Addgene) and designated as LV-shCTSC (mice), LV-shCTSC (human), and LV-shcontrol. "LV-shcontrol" is a non-target shRNA control. The vector "pLKO.1-puro non-Target shRNA Control Plasmid DNA" (purchased from Sigma, SHC016) contains an shRNA insert that does not target any known genes from any species. Short hairpin RNAs (shRNAs) sequences were: shCTSC (human), 5'-GCTGCTACTCATTTGCTTCTA-3'.

Lentiviral vectors encoding the mice CTSC genes were constructed in FUW-teto (Addgene) and designated as LV-CTSC. An empty vector was used as the negative control and was designated as LV-control. Concentrated lentivirus was transfected into the CRC cells with a multiplicity of infection (MOI) ranging from 30 to 50 in the presence of polybrene (6 µg/ml). Seventy-two hours after infection, CRC cells were selected for 2 weeks using 2.5 µg/ml puromycin (OriGene). Selected pools of knockdown and overexpression cells were used for the following experiments.

In vitro invasion and migration assay. For the migration and invasion assay, a 24-well chamber with an 8 µm pore filter (Corning Corporation, USA) was used. For migration assay, 5×10^5 cells were seeded into the upper chamber in a serum-free medium. For invasion assay, 5×10^5 cells were implanted in the top chamber with Matrigel (Corning

Corporation, USA). After 24–48 hours, the cells were fixed with 95% ethanol and stained with crystal violet. The mean of triplicate assays for each experimental condition was used.

Real-time PCR. Total RNA was extracted using TRIzol Reagent (Invitrogen), and reverse transcription was performed using the Advantage for RT-PCR Kit (Takara) according to the manufacturer's instructions. For the real-time PCR analysis, aliquots of double-stranded cDNA were amplified using an SYBR Green PCR Kit (Applied Biosystems). For the clinical tissue samples, the fold change of the target gene was determined by the following equation: $2^{-\Delta\Delta Ct}$ ($\Delta\Delta Ct = \Delta Ct^{\text{tumor}} - \Delta Ct^{\text{nontumor}}$). This value was normalized to the average fold change in the normal colon tissues, which was defined as 1.0. All reactions were performed in duplicate. The primer sequences for CTSC sense were 5'-CCAACTGCACCTATCTTGACC-3'; CTSC antisense was 5'-AAGGCAAACCACTTGTAGTCATT-3'.

Western blotting. For the western blotting assay, the lysed cells' proteins were separated on SDS-PAGE and transferred onto a polyvinylidene difluoride membrane. The nonspecific binding was blocked with 10% non-fat milk for one hour. The membranes were incubated with specific antibody overnight at 4°C. β -actin was used on the same membrane as a loading control. Antibody against CTSC (ab199109) expression was purchased from Abcam. Antibody against β -actin (A1978) was purchased from Sigma. The membranes were then washed with PBS 3 times and incubated with an HRP-conjugated secondary antibody. Proteins were visualized using an Immobilon™ Western Chemiluminescent HRP substrate (Millipore, USA).

Immunohistochemistry. This study was authorized by the Shaanxi Provincial People's Hospital Ethics Committee, and informed consent was signed and based on the 1975 Declaration of Helsinki's ethical criteria. Furthermore, human subjects' private rights were always respected. A tissue microarray was created using CRC specimens and matched adjacent tissues (Shanghai Biochip Co, Ltd. Shanghai, China). CTSC (Abcam, ab199109), CD11b (Abcam, ab6640), F4/80 (Abcam, ab6640), CD163 (Abcam, ab182422), and CD8 (Abcam, ab4055) expression was detected by immunohistochemistry (IHC). IHC was carried out on 4 µm thick paraffin-embedded slices that had been normally treated. Images were captured using an Olympus light microscope with a DP70 digital camera (Olympus, Japan).

Analyses were performed by two independent observers who were blinded to the clinical outcome. The level of immunostaining was graded on a scale of 0 to 3: 0 (negative), 1 (weak), 2 (medium), or 3 (strong). On a scale of 0 to 4, the proportion of positive cells was rated as follows: 0 (negative), 1 (1–25%), 2 (26–50%), 3 (51–75%), or 4 (76–100%). The final immuno-activity scores were determined by multiplying the two values above, yielding an overall score ranging from 0 to 12. If the final score ranged from 0 to 3, the case was deemed "negative", and if the final score ranged from 4 to 12, it was deemed "positive" [18].

Animal experiments. Our implantation tests were approved by the Shaanxi Provincial People's Hospital Ethics Committee. Under anesthesia, luciferase-labeled mouse CRC cells (4.0×10^6) were injected into the cecal wall of nude or C57BL/6 mice ($n=10$ for each group). The IVIS-100 Imaging System was used to track tumor development and metastasis on a weekly basis. During the tests, every attempt was taken to keep the animals as pain-free as possible. The mice were euthanized at 9 weeks by administering excessive pentobarbital sodium (100 mg/kg, Merck, Darmstadt, Germany) for anesthesia, and the livers and lungs were collected and histologically examined [18].

***In vivo* metastatic model and bioluminescent imaging.** Our implantation tests were under the approval of the ethics of the Committee of Shaanxi Provincial People's Hospital. All efforts were made to minimize the animals' suffering during the experiments. C57BL/6 mice (5 weeks old) were housed under standard conditions and cared for according to the institutional guidelines for animal care. A metastatic colorectal cancer model in mice was established according to the existing protocol. Luciferase-labeled mouse CRC cells (4.0×10^6) were injected into the cecal wall in mice under anesthesia ($n=10$ for each group). Briefly, the caecum was gently exteriorized and placed on a scalpel holder, flattened, and stabilized with forceps. This maneuver is crucial to prevent leakage of tumor cells into the cecal lumen or peritoneal cavity. A volume of 100 μ l (4.0×10^6) cells was injected into the cecal wall. Then, the caecum was returned to the peritoneal cavity, peritoneum and skin were closed by running sutures and wound clips.

Luciferase lentivirus was purchased from Shanghai Genechem Co., Ltd. Concentrated luciferase lentivirus was transfected into the CRC cells with a multiplicity of infection (MOI=50) in the presence of polybrene (6 μ g/ml). Seventy-two hours after infection, CRC cells were selected for 2 weeks using 2.5 μ g/ml puromycin (OriGene). Then we tested the luciferase infection efficiency. In a 96-well plate, we set up 4 gradient dilution cells (each hole is spaced at a certain distance to prevent mutual interference). Then, 5 μ l D-luciferin was added to each hole, and the signal value of each well was measured by a multifunctional enzyme marker. If the cell density was positively correlated with the signal value, indicated luciferase transfection success.

The *in vivo* tumor formation and metastases were imaged by bioluminescence. D-luciferin (Xenogen, Hopkinton, MA, USA) at 100 mg/kg was injected intraperitoneally into the mice, and bioluminescence was detected using an IVIS 100 Imaging System (Xenogen). After acquiring photographic images of each mouse, luminescent photos were captured using various (1–60 seconds) exposure times. The resulting grayscale photographic and pseudocolored luminescent images were automatically superimposed using the IVIS Living Image (Xenogen) software. This superimposition was performed to facilitate the matching of the observed luciferase signal with its location on the mouse. The survival of

the mice was recorded daily. After 10 weeks, the mice were sacrificed, and their lungs were dissected and prepared for standard histological examination.

At the 9 weeks, the mice were sacrificed by injecting excessive pentobarbital sodium for anesthesia (100 mg/kg, Merck, Germany), and the livers and lungs were collected and underwent histological examination.

Preparation of single-cell suspensions. Mice were perfused with PBS and anesthetized, and tumors were dissected using a clean razor. Then, the tumor tissues were digested with DNase I (20 mg/ml, Sigma-Aldrich) and collagenase IV (1.5 mg/ml, Sigma-Aldrich) and placed on a table concentrator at 37°C for one hour. At the end of one hour, we filtered the dissociated cells through 70 μ m pore filters rinsed with fresh media. The 1 \times red cell lysis was added to the tissues and incubated for 5 minutes to lysis the red blood cell, followed by another rinse.

Flow cytometric analysis. Cells were incubated with anti-mouse CD16/CD32 purified antibody (#101302, clone 93, Biolegend) for 10 minutes to block nonspecific antibodies. Then, the cells were stained with fluorophore-conjugated antibodies. Matched isotype antibodies were used as a control. Antibodies against CD45 (PE, #103105), CD11b (FITC, #101205), CD45 (PE/Cy7, #103113), Ly-6G/Ly-6C (Gr-1) (PE, #108407), CD3 (FITC, #100203), CD8 (PE, #100707), F4/80 (PE/Cy7, #123113), were purchased from BioLegend. Data were analyzed by Flowjo_V10 software (TreeStar, Ashland, OR, USA).

Statistical analysis. SPSS software was used to calculate the statistics (version 20.0). The χ^2 test was used to examine p values for categorical variables, while the Student's test was used to investigate p values for quantitative data. The Kaplan-Meier technique was used to assess the recurrence and survival data. For both univariate and multivariate analyses, the Cox proportional hazards model was utilized. When $p < 0.05$, differences were judged statistically significant [18].

Results

Elevated CTSC is associated with poor prognosis in CRC patients. We used RT-PCR to evaluate CTSC expression in a cohort of 90 matched CRC and adjacent nontumor tissues, as well as 20 normal colon epithelial specimens, to determine the clinical significance of CTSC expression in CRC. CTSC expression is significantly higher in CRC tissues than in adjacent non-tumor tissues and normal colon tissues (Figure 1A). Furthermore, CTSC expression was higher in patients with recurrence or metastasis than in patients without recurrence or metastasis (Figures 1B, 1C). To investigate the role of CTSC in human CRC metastasis, immunohistochemistry was used to measure its expression in 20 paired primary and metastatic CRC tissues. CTSC expression was shown to be greater in metastatic CRC tissues than in primary CRC samples and nontumor tissues (Figure 1D). We then aimed to profile CTSC expression in 222 samples

with a CRC tissue microarray. IHC staining revealed CTSC expression was significantly higher in CRC tissues than in surrounding nontumor tissues in the CRC cohort (Figure 1E). We discovered that elevated CTSC expression was linked to tumor differentiation, invasion, lymph node metastasis, and the AJCC stage (Table 1). Patients with high CTSC expression had a shorter overall survival rate and a greater recurrence rate than patients with low CTSC expression, according to the survival analysis (Figure 1F). CTSC expression was found to be an independent predictor of the patient's high recurrence rate and poor overall survival in the multivariate Cox proportional hazards model (Table 2). Based on the findings, CTSC is a prognostic biomarker for human CRC.

Elevated expression of CTSC promotes CRC metastasis.

To examine the contribution of CTSC in CRC progression, we evaluated the effect of CTSC on cell migration in gain-of-function experiments *in vitro*. CTSC expression failed to promote migration in SW480 cells *in vitro* (Figure 2A). Next, we injected SW480-CTSC and its corresponding control cells into the tail of nude mice. It showed that the overexpression of CTSC did not alter the metastasis rate of SW480

cells (Figure 2B). Thus, these results indicated that CTSC is not essential for CRC metastasis in the immunosuppressive microenvironment.

Chronic inflammation plays an important role in developing CRC [19]. We postulated that CTSC promoted CRC metastasis by changing the immune microenvironment. To explore the contribution of CTSC in CRC progression, we established the stable cell line MC38-CTSC by lentiviral transduction. We injected MC38-CTSC cells and their corresponding control cells into the cecal wall in C57BL/6 mice and monitored the metastasis ability of the xenografted cells. *In vivo* metastatic analysis showed that CTSC overexpression boosted lung and liver metastasis capacity by increasing metastatic rate and metastatic nodules' number in MC38 cells group mice. In addition, CTSC can shorten the overall survival of C57BL/6 mice (Figures 2C–2H). These results suggested that overexpression of CTSC facilitated CRC metastasis in immunocompetent mice.

CTSC promotes CRC metastasis through the recruitment of MDSCs and TAMs. We investigated the cellular immune response to explore the underlying mechanisms

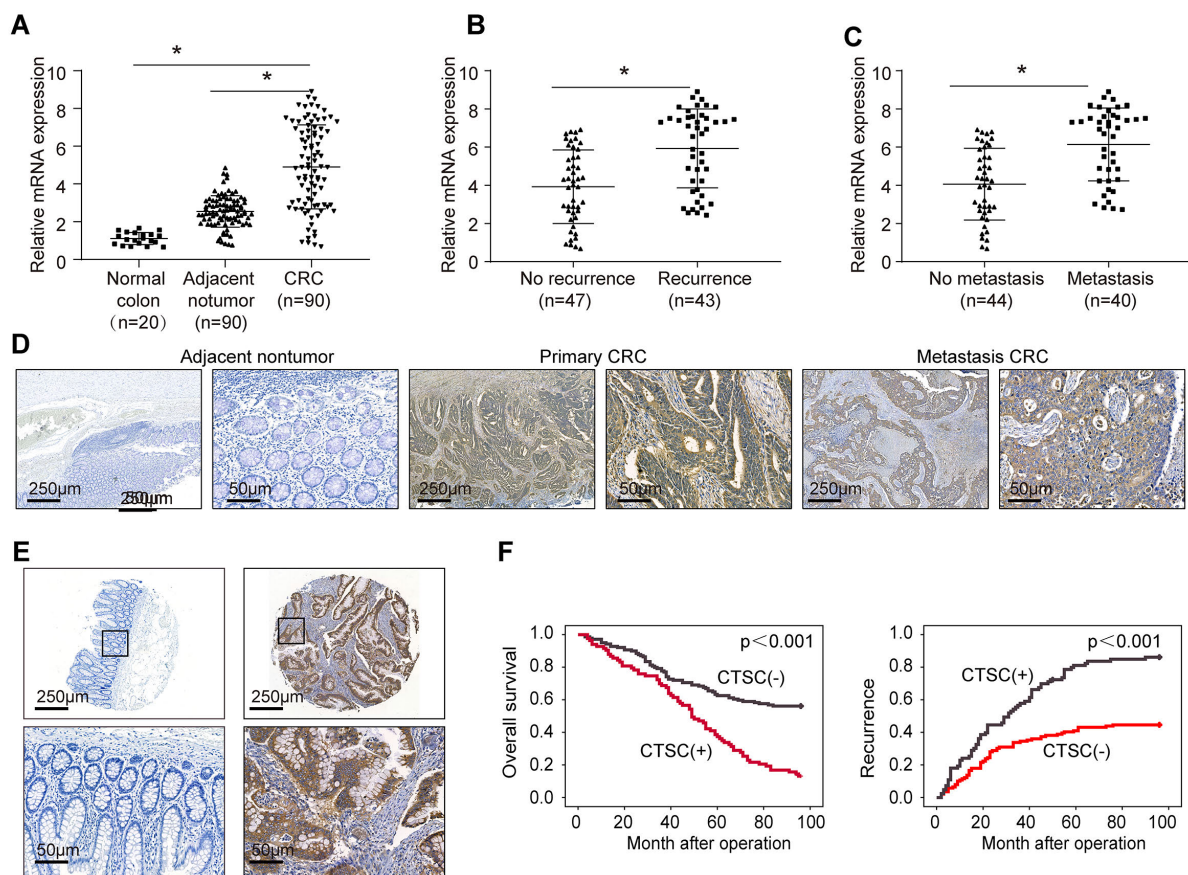


Figure 1. Elevated CTSC is associated with a poor prognosis in colorectal cancer. **A**). Real-time PCR analysis of *CTSC* mRNA expression in normal colon tissue (n=20), 90 paired CRC tissues, and adjacent nontumorous tissues. **B**). Relative *CTSC* mRNA expression in CRC patients with (n=43) or without (n=47) recurrence. **C**). Relative *CTSC* mRNA expression in CRC patients with (n=40) or without (n=44) metastasis. **D**) *CTSC* protein expression in paired adjacent nontumor, primary CRC tissues, and metastasis CRC by IHC. **E**) IHC staining of *CTSC* in adjacent nontumorous tissues and primary CRC tissues in the CRC cohort. **F**) Kaplan-Meier analysis of the correlation of *CTSC* expression with overall survival and recurrence.

by which CTSC signaling promotes CRC metastasis. Then, we used the immunocompetent C57BL/6 mice for *in vivo* study. Flow cytometric was applied to detect the percentage of tumor-infiltrating immune and inflammatory cells in separated tumors. The transplantation of MC38-CTSC cells significantly increased MDSCs (marked by CD45+/CD11b/Gr1+) and TAMs (marked by CD45+/CD11b+/F4/80+) accumulation, while decreased infiltration of CD8+T cells (marked by CD45+/CD3+/CD8+) (Figure 3A). Similarly, IHC staining exhibited that CTSC overexpression boosted MDSCs and TAMs infiltration and impaired CD8+T cell recruitment (Figure 3B).

Furthermore, we detected the expression of CD11b and CD163 in a cohort of human CRC tissues, and representative images are shown in Figure 3C. Correlation analyses showed that CTSC positively correlated with CD11b or CD163 (Figure 3D). Kaplan-Meier’s analysis showed that CRC patients with positive CD11b or CD163 expression showed poorer overall survival and elevated recurrence rates than patients with negative CD11b or CD163 expression. Furthermore, we found that positive coexpression of either CSTC/CD11b or CTSC/CD163 had the lowest survival rate and the highest risk recurrence rate (Figure 3E).

CTSC overexpression induces MDSCs and TAMs chemotaxis through CSF1 in CRC. To study the underlying mechanism of CTSC recruit immunosuppressive cells, we constructed SW480-CTSC and SW480-control stable cell lines by lentivirus. We compared transcriptome changes in SW480-CTSC and SW480-control cells using an Affymetrix PrimeView Human Gene Expression Array.

Table 1. Correlation between CTSC expression and clinicopathological characteristics in cohort of human CRC tissues.

Clinicopathological variables	Tumor CTSC expression		p-value
	Negative (n=139)	Positive (n=83)	
Age			
≤50	70	34	0.175
>50	69	49	
Gender			
female	66	34	0.345
male	73	49	
Tumor size			
≤5 cm	67	30	0.08
>5 cm	72	53	
Tumor differentiation			
well or moderate	107	49	0.005
poor	32	34	
Tumor invasion			
T1–T3	117	59	0.02
T4	22	24	
Lymph node metastasis			
absent	87	37	0.009
present	52	46	
Distant metastasis			
absent	117	66	0.378
present	22	17	
AJCC stage			
I–II	87	35	0.003
III–IV	52	48	

Table 2. Univariate and multivariate analysis of factors associated with survival and recurrence in cohort of human CRC.

Clinical Variables	Time to Recurrence		Overall Survival	
	HR (95% CI)	p-value	HR (95% CI)	p-value
Univariate analysis				
Age (≤50 vs. >50)	0.937 (0.666–1.317)	0.707	0.942 (0.670–1.324)	0.729
Gender (female vs. male)	0.881 (0.627–1.238)	0.465	0.913 (0.650–1.284)	0.603
Tumor size (≤5 cm vs. >5 cm)	1.304 (0.921–1.845)	0.135	0.739 (0.522–1.047)	0.086
Tumor differentiation (well/moderate vs. poor)	0.165 (0.115–0.238)	<0.001	0.156 (0.108–0.225)	<0.001
Tumor invasion (T1–3 vs. T4)	0.290 (0.20–0.422)	<0.001	0.296 (0.204–0.403)	<0.001
Lymph node metastasis (absent vs. present)	0.096 (0.063–0.146)	<0.001	0.096 (0.064–0.146)	<0.001
Distant metastasis (absent vs. present)	0.098 (0.062–0.153)	<0.001	0.101 (0.065–0.156)	<0.001
AJCC stage (I–II vs. III)	0.086 (0.056–0.113)	<0.001	0.078 (0.051–0.121)	<0.001
CTSC expression (negative vs. positive)	0.363 (0.257–0.513)	<0.001	0.368 (0.269–0.520)	<0.001
Multivariate analysis				
Tumor differentiation (well/moderate vs. poor)	0.923 (0.575–1.480)	0.739	0.898 (0.543–1.393)	0.561
Tumor invasion (IT1–3 vs. T4)	0.737 (0.487–1.114)	0.148	0.779 (0.516–1.177)	0.236
Lymph node metastasis (absent vs. present)	0.417 (0.145–1.196)	0.104	0.424 (0.171–1.1053)	0.064
Distant metastasis (absent vs. present)	0.248 (0.144–0.430)	<0.001	0.277 (0.164–0.466)	<0.001
AJCC stage (I–II vs. III)	0.298 (0.10–0.885)	0.029	0.269 (0.105–0.692)	0.006
CTSC expression (negative vs. positive)	0.457 (0.319–0.655)	<0.001	0.506 (0.353–0.725)	<0.001

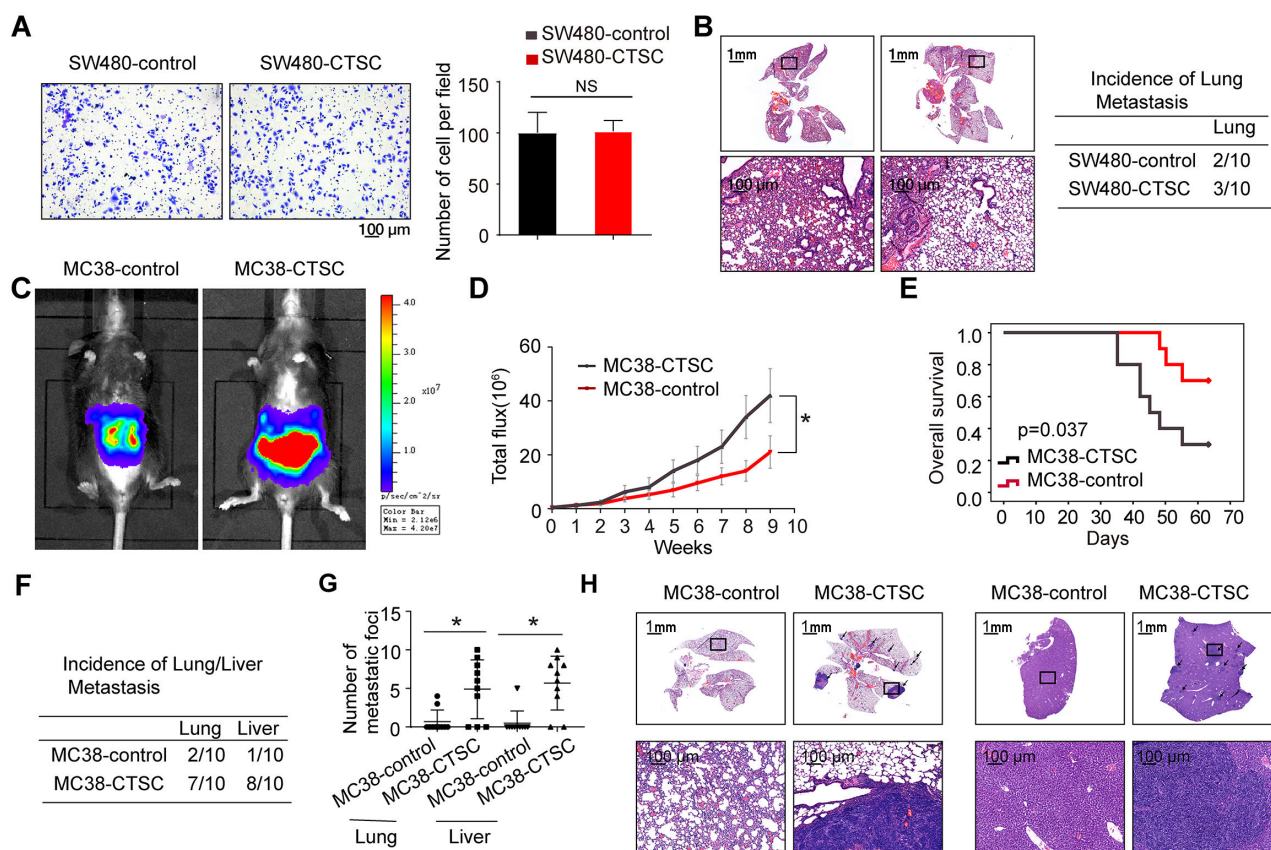


Figure 2. CTSC upregulation promotes CRC metastasis in immunocompetent mice. **A)** Transwell assay the migration rate of SW480-CTSC and its control cells. **B)** Representative HE staining of lung tissues from two groups is shown. **C–H)** The indicated CRC cell lines were injected into the cecal wall of C57BL/6 mice under anesthesia. **C)** Bioluminescent images. **D)** Bioluminescent signals. **E)** Overall survival. **F)** The incidence of liver and lung colonization. **G)** The number of liver and lung colonization. **H)** Representative HE staining of lung tissues and liver tissues from the different groups is shown. The scale bars represent 1 mm (low magnification) and 100 μ m (high magnification). All the data are shown as the means. * $p < 0.05$ ** $p < 0.01$

Overexpression of CTSC increased the expression of several metastasis-related genes, such as CSF1, CXCL5, and CXCL3 (Supplementary Table S1). Among these genes, CSF1 was the most upregulated gene. CSF1, a ligand for the CSF1 receptor (CSF1R), plays a pivotal role in monocyte/macrophage generation, survival, and function [19]. Previously, a critical role of systemic CSF1 expression was reported in HCC patients with metastasis [18]. Considering the important role of CSF1 in cancer progression, we focused on CSF1 for further study. Western blot and RT-qPCR showed that CTSC overexpression markedly increased CSF1 expression in SW480 cells, while CTSC knockdown in SW620 cells significantly decreased CSF1 expression (Figures 4A, 4B).

To study the function of CSF1 in CRC metastasis, we downregulated CSF1 in MC38-CTSC cells by lentivirus and generated the cecum orthotopic tumor implantation model in immune-competent C57BL/6 mice. *In vivo* study showed that CSF1 knockdown can significantly reduce lung and liver metastasis while prolonging the survival of the MC38-CTSC-shCSF1 group compared to the MC38-CTSC-shcontrol

(Figures 4C–4G). Moreover, IHC staining analysis exhibited that knockdown of CSF1 expression in MC38-CTSC cells can significantly reduce the infiltration rate of MDSCs and TAMs while increasing the CD8⁺ T cells infiltration (Figure 4H).

Depletion of MDSCs or TAMs decreases CTSC-mediated CRC metastasis. To examine whether MDSCs infiltration was required for CTSC-mediated CRC metastasis, we established a cecal metastasis model using MC38-CTSC cells in C57BL/6 mice. The anti-Gr1 antibody, clone RB6-8C5, a well-characterized anti-Gr1 antibody, was used to deplete MDSCs. CTSC overexpression enhanced lung and liver metastasis and decreased the survival time of C57BL/6 mice in an *in vivo* metastasis experiment. In the MC38-CTSC cells group, anti-Gr1 decreased the burden of lung and liver metastases while also increasing overall survival time (Figures 5A–5E). To study the role of TAMs recruitment in CTSC-mediated CRC metastasis, we depleted TAMs with clodronate liposomes [20]. *In vivo* metastasis assay showed that clodronate liposomes treatment significantly reduced

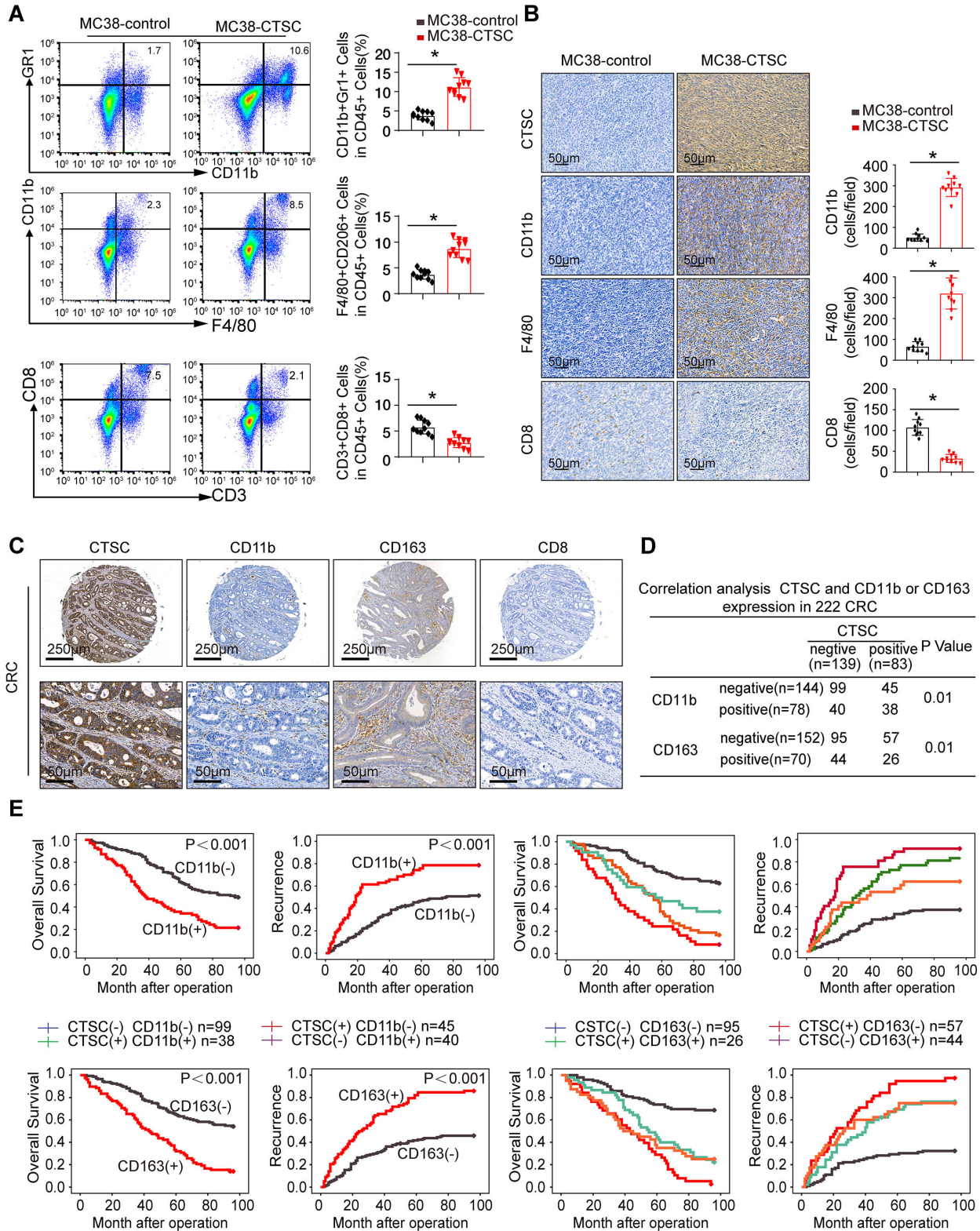


Figure 3. CTSC promotes CRC metastasis through the recruitment of MDSCs and TAMs. **A)** The infiltration of immune cells in the two groups was analyzed by flow cytometry. **B)** The expression of CTSC, CD11b, F4/80, and CD8 in two groups was analyzed by IHC. **C)** IHC staining showed CTSC, CD11b, CD163, and CD8 expression in the CRC cohort. **D)** The correlation between CTSC expression and CD11b or CD8 expression in the CRC cohort. **E)** The correlation between CTSC expression, intratumoral MDSCs or TAMs infiltration, and recurrence and overall survival in the CRC cohort.

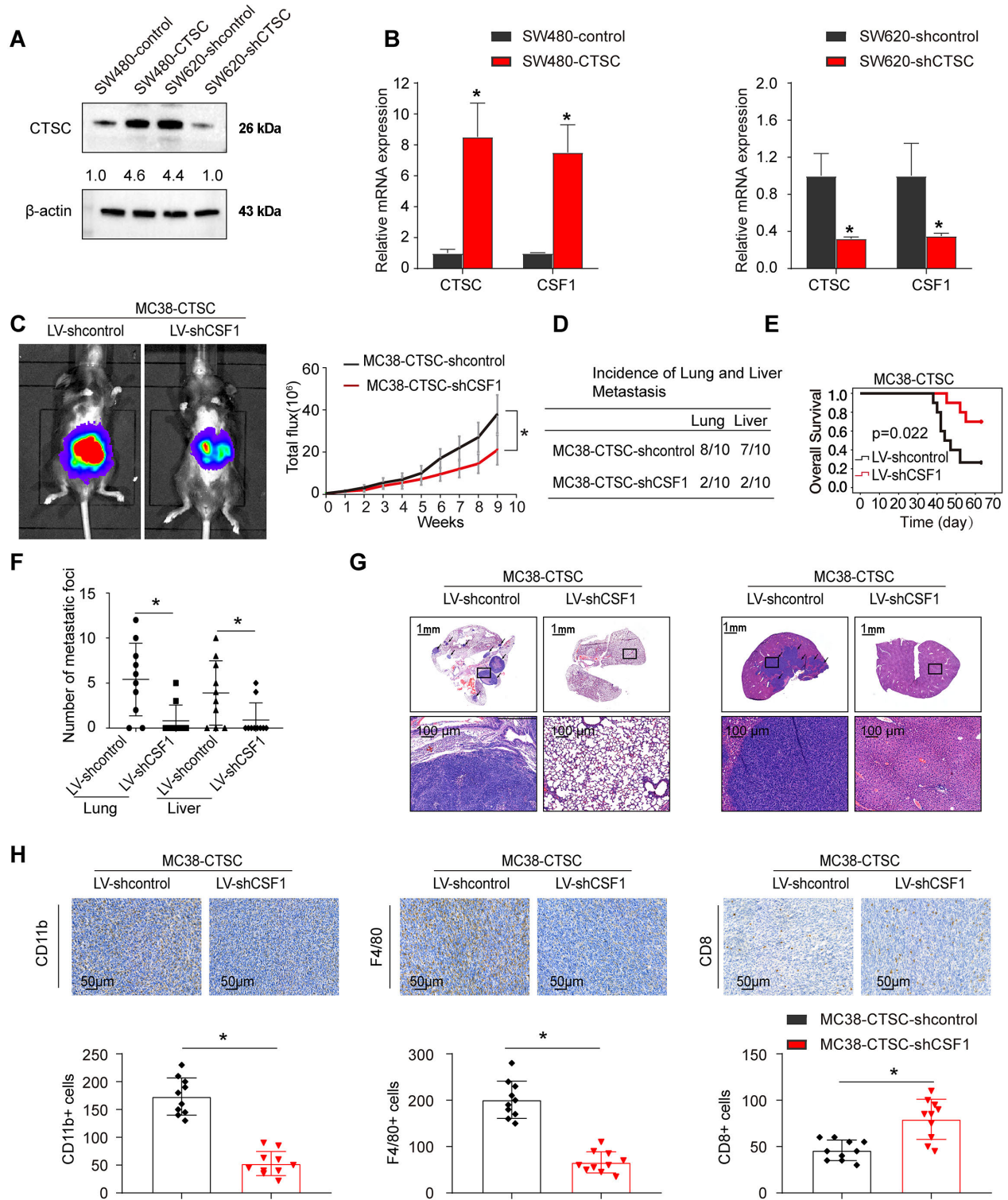


Figure 4. CTSC overexpression induces MDSCs and TAMs chemotaxis through CSF1 in CRC. **A)** CTSC expression in the indicated cell by western blot. **B)** CTSC and CSF1 expression in the indicated cell by real-time PCR analysis. **C–G)** CSF1 knockdown can reduce CTSC-mediated CRC metastasis. **C)** Bioluminescence images and Bioluminescence signals. **D)** The number of lungs and liver colonization. **E)** Overall survival. **F)** The incidence of lung and liver colonization. **G)** HE staining. **H)** The infiltration of MDSCs, TAMs, and CD8 in two groups was analyzed by IHC. All the data are shown as the mean \pm S.D. * $p < 0.05$

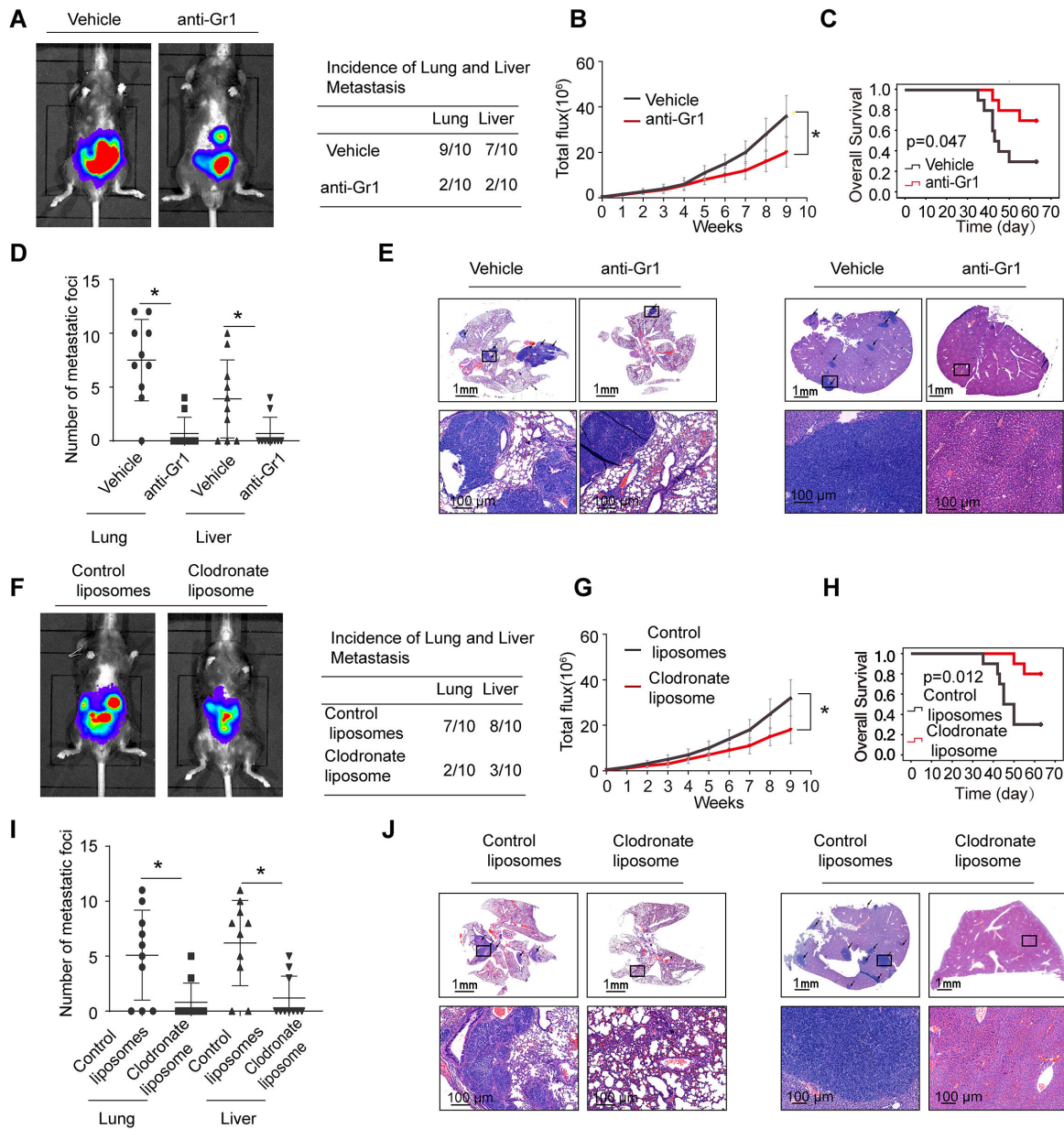


Figure 5. Depletion of MDSCs or TAMs can decrease MC38-CTSC cell-induced CRC metastasis. A–E) *In vivo* administration of anti-Gr1 neutralizing monoclonal antibody (clone RB6-8C5, 200 µg/mouse, i.p., every three days) or Vehicle until treatment endpoint. Anti-Gr1 can significantly inhibit CTSC-mediated CRC metastasis. A) Bioluminescence images and the incidence of lung and liver metastasis. B) Bioluminescence signals. C) Overall survival. D) The numbers of lung and liver nodules. E) Representative HE staining. F–J) *In vivo* administration of clodronate liposomes or control liposomes until treatment endpoint. Clodronate liposomes can significantly inhibit CTSC-mediated CRC metastasis. F) Bioluminescence images and the incidence of lung and liver metastasis. G) Bioluminescence signals. H) Overall survival. I) The numbers of lung and liver nodules. J) Representative HE staining. The scale represents 1 mm (low magnification) and 100 µm (high magnification). All the data are shown as the mean ± S.D. *p<0.05

liver and lung metastasis burden and prolonged the overall survival time in the MC38-CTSC groups (Figures 5F–5J). Anti-Gr1 and clodronate liposome treatment remarkably reduced MDSCs and TAMs infiltration, respectively. Together, these results strongly suggest that CTSC boosted CRC metastasis by recruiting MDSCs and TAMs.

The combined application of CTSC inhibitor AZD7986 and anti-PD-L1 dramatically blocks CTSC-mediated CRC metastasis. Given the pivotal role and clinical relevance of CTSC in CRC metastasis, we wondered whether targeting CTSC could be an effective strategy in the treatment of metastatic CRC. Thus, we established a cecal metastasis

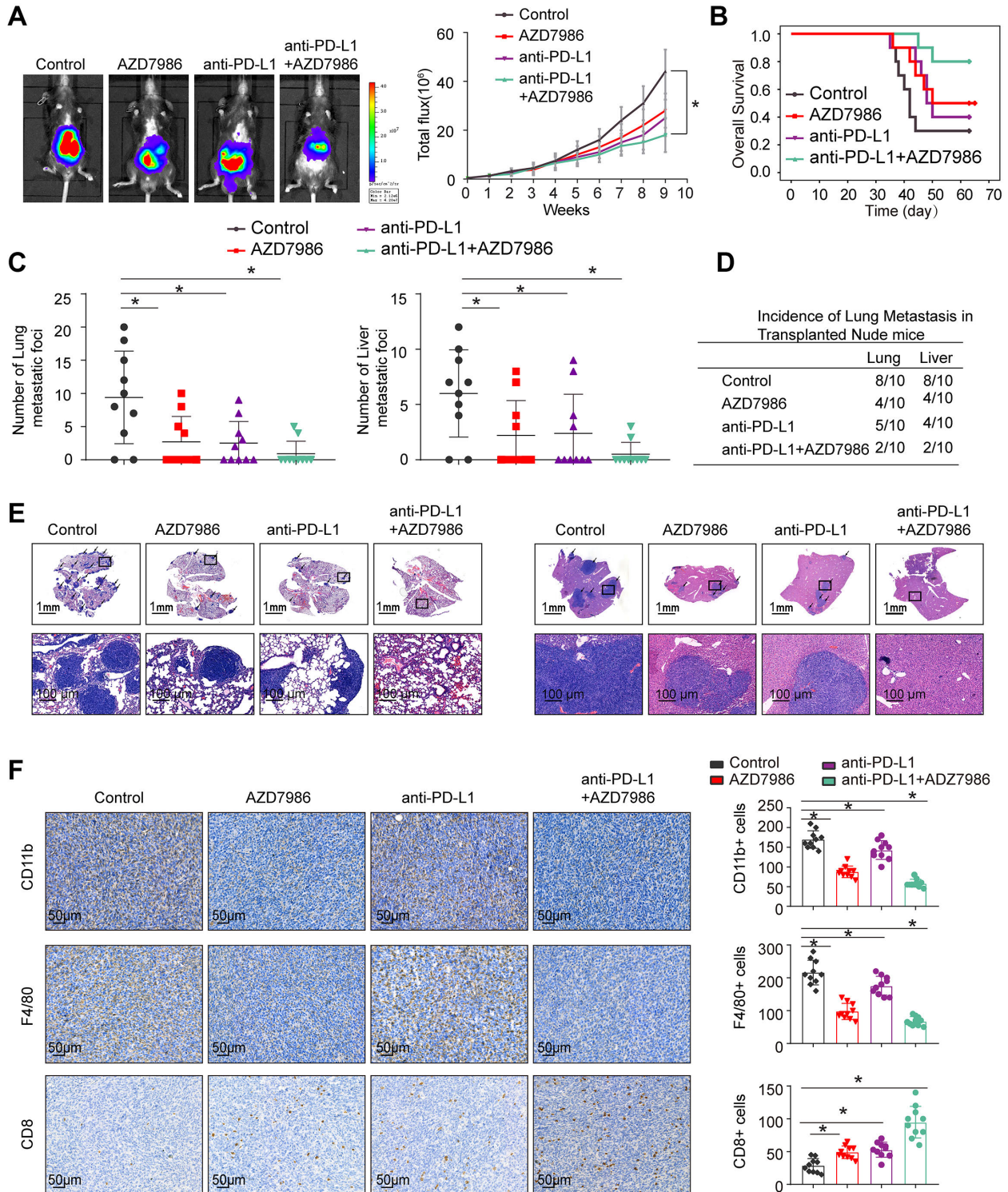


Figure 6. Combined CTSC inhibitor AZD7986 and anti-PD-L1 dramatically block CTSC-promoted CRC metastasis. **A–E)** One week after injection of MC38-CTSC cells, mice were divided into four groups and treated with vehicle, AZD7986 or/and PD-L1 antibody ($n=10$ mice/group) respectively, until treatment endpoint. *In vivo* assays showed that combined PD-L1 antibody and AZD7986 can almost inhibit CRC metastasis. **A)** Representative bioluminescent images and bioluminescent signals in the indicated group. **B)** Overall survival in the indicated group. **C)** The numbers of lung and liver nodules in the indicated group. **D)** The incidence of lung and liver nodules in the indicated group. **E)** Representative HE staining of lung and liver tissues. **F)** IHC staining detected the expression of CD11b, F4/80, and CD8 in the indicated group. All the data are shown as the mean \pm S.D. * $p < 0.05$

model using MC38-CTSC cells in C57BL/6 mice. AZD7986 is a second-generation CTSC inhibitor and a therapeutic candidate for neutrophil-induced inflammatory disease, such as chronic obstructive pulmonary disease [21, 22]. *In vivo* metastatic assays revealed that AZD7986 remarkably reduced lung and liver metastasis incidence compared with isotype control, whereas contributing to prolonged overall survival in MC38-CTSC cells in C57BL/6 mice (Figures 6A–6E). In addition, IHC staining showed the infiltration of MDSCs and TAMs significantly reduced, whereas the percentage of CD8+ T cells increased in AZD7986-treated MC38-CTSC orthotopic tumors (Figure 6F).

PD-1/PD-L1 immune checkpoint signaling has been proven as a promising target in CRC. However, the low response rate to the anti-PD-1/PD-L1 therapies emphasizes the potential of synergy combination strategies. Since MDSCs and TAMs are known negative regulators of immunotherapy efficacy, we wondered whether AZD7986, which inhibited the recruitment of the MDSCs and TAMs, can enhance CRC response to the anti-PD-1 blockade. *In vivo* study showed the combination treatment remarkably reduced the incidence of lung and liver metastasis incidence, whereas prolonged overall survival of the mice compared to AZD7986 or anti-PD-1 alone (Figures 6A–6E). Moreover, IHC staining showed a significant reduction of MDSCs and TAMs, while increased infiltrating of CD8+ T cells in the combination treatment group (Figure 6F). These results indicated that combined therapy with AZD7986 and anti-PD-1 markedly suppressed CTSC-induced CRC metastasis by abrogation of MDSCs and TAMs immunosuppression, and triggered cytotoxic CD8+T cell infiltration.

Discussion

A better understanding of the oncogenic gene may be beneficial to understand the molecular profiling in CRC metastasis and developing more potent combination-based therapies. In this study, we identified CTSC as a poor prognostic indicator for CRC metastasis. CTSC was positively associated with a higher metastasis rate, a more aggressive tumor phenotype, and shorter overall survival. Moreover, CTSC overexpression promoted CRC cells' metastasis by recruiting both MDSCs and TAMs. This evidence indicated the key role of CTSC in promoting CRC metastasis.

Immune invasion is frequently associated with PD-1/PD-L1 amplification and the infiltration of immunosuppressive cells [22–24]. MDSCs and TAMs are believed to play pivotal roles in immune escape and are involved in CRC progression [25–27]. The CSF1/CSF1R pathway promotes cancer progression and is essential for the infiltration of TAMs and MDSCs [28]. In line with these results, CSF1R monoclonal antibody showed promising antitumor activity and acceptable safety profile in various tumors, including CRC [29]. In this study, we found that CTSC unregulated CSF1 expression, which promoted the recruitment of

MDSCs and TAMs to the CRC tumor niche. Moreover, *in vivo* study showed that downregulation of CSF1 can inhibit CTS-mediated CRC metastasis, as well as significantly impede the infiltration of MDSCs and TAMs. These results indicated that CSF1-mediated MDSCs and TAMs infiltration played a key role in CTSC-induced CRC metastasis.

Although PD-1/PD-L1 immune checkpoint inhibition has demonstrated a positive therapeutic impact, only a small percentage of CRC patients treated with it have long-term responses [30]. As a result, combined techniques to improve CRC therapy effectiveness have become critical. Anti-PD-1/anti-PD-L1 combined with anti-CTLA4 drugs, locoregional treatments, or VEGF/VEGFR inhibitors, for example, boosts anti-tumor immunity synergistically [31–33]. These findings suggested that anticancer drugs that stimulate tumor immunity, when combined with anti-PD-1/anti-PD-L1 antibodies, might provide show encouraging effects. Among the many variables that might cause immune evasion, infiltrated suppressive immune cells are the most important [16]. As a result, inhibiting invading immune cells might be a potential way to increase the efficacy of checkpoint blockade therapy [27]. These researches lay the groundwork for CRC combination treatment. In this context, we hypothesized that inhibiting the CSTC pathway might increase the efficiency of immunotherapy treatment by modulating the immunological characteristics of CRC. AZD7986 is a second-generation CTSC inhibitor that might be used to treat diseases caused by neutrophils, such as chronic obstructive pulmonary disease [21–22]. AZD7986 can also significantly reduce breast cancer brain metastases [11]. In this research, we discovered that combining the CSTC inhibitor AZD7986 with the PD-L1 antibody significantly reduced CTSC-mediated CRC metastasis and increased mouse survival time when compared to a vehicle or a single drug.

In summary, we report a novel function of CTSC in CRC metastasis. CTSC overexpression facilitated the recruitment of MDSCs and TAMs to the tumor niche by upregulated CSF1 expression, thereby contributing to CRC metastasis. Combined targeting of CTSC and anti-PD-L1 largely suppressed CRC metastasis. Our works indicated that CTSC was a potential prognostic biomarker for CRC, and targeting the oncogenic loop may provide a promising therapeutic strategy for CTSC-mediated CRC metastasis.

Acknowledgments: This study was supported by the Open Project Program of the State Key Laboratory of Cancer Biology (Fourth Military Medical University) (No.CBSKL2022KF15), National Natural Science Foundation of China (No.82203521), Natural Science Basic Research Program of Shaanxi (No. 2022JQ-775), Health Scientific Research project of Shaanxi Province (No.2022E020), Young Talents Fund of Association for Science and Technology in Shaanxi (No. SWYY202210), Scientific and Technological Talents support Program Foundation of Shaanxi Provincial People's Hospital (No.2021JY-05), Incubation Fund Program of Shaanxi Provincial People's Hospital (No.2021YJY-12), Social Development Field

in General Project of Key Research and Development Program of Shaanxi Province (No. 2021SF-306).

References

- [1] SIEGEL RL, MILLER KD, JEMAL A. Colorectal cancer statistics 2020. *CA Cancer J Clin* 2020; 70: 7–30. <https://doi.org/10.3322/caac.21590>
- [2] DEKKER E, TANIS PJ, VLEUGELS JLA, KASI PM, WAL-LACE MB. Colorectal cancer. *Lancet* 2019; 394: 1467–1480. [https://doi.org/10.1016/S0140-6736\(19\)32319-0](https://doi.org/10.1016/S0140-6736(19)32319-0)
- [3] CANON J, REX K, SAIKI AY, MOHR C, COOKE K et al. The clinical KRAS(G12C) inhibitor AMG 510 drives anti-tumour immunity. *Nature* 2019; 575: 217–23. <https://doi.org/10.1038/s41586-019-1694-1>
- [4] ADKISON AM, RAPTIS SZ, KELLEY DG, PHAM CTN. Dipeptidyl peptidase I activates neutrophil-derived serine proteases and regulates the development of acute experimental arthritis. *J Clin Invest* 2002; 109: 363–71. <https://doi.org/10.1172/JCI13462>
- [5] KORKMAZ B, CAUGHEY GH, CHAPPLE I, GAUTHIER F, HIRSCHFELD J et al. Therapeutic targeting of cathepsin C: from pathophysiology to treatment. *Pharmacol Ther* 2018; 190: 202–36. <https://doi.org/10.1016/j.pharmthera.2018.05.011>
- [6] TURK V, STOKA V, VASILJEVA O, RENKO M, SUN T et al. Cysteine cathepsins: from structure, function and regulation to new frontiers. *Biochim Biophys Acta* 2012; 1824: 68–88. <https://doi.org/10.1016/j.bbapap.2011.10.002>
- [7] PHAM CT, IVANOVICH JL, ZAPTIS SZ, ZEHNBAUER B, LEY TJ. Papillon-Lefevre syndrome: correlating the molecular, cellular, and clinical consequences of cathepsin C/dipeptidyl peptidase I deficiency in humans. *J Immunol* 2004; 173: 7277–7281. <https://doi.org/10.4049/jimmunol.173.12.7277>
- [8] HART TC, HART PS, MICHALEC MD, ZHANG Y, FIRATLI E et al. Haim-Munk syndrome and Papillon-Lefevre syndrome are allelic mutations in cathepsin C. *J Med Genet* 2000; 37: 88–94. <https://doi.org/10.1136/jmg.37.2.88>
- [9] KHAKET TP, KWON TK, KANG SC. Cathepsins: Potent regulators in carcinogenesis. *Pharmacol Ther* 2019; 198: 1–19. <https://doi.org/10.1016/j.pharmthera.2019.02.003>
- [10] RUFFELL B, AFFARA NI, COTTONE L, JUNANKAR S, JOHANSSON M et al. Cathepsin C is a tissue-specific regulator of squamous carcinogenesis. *Genes Dev* 2013; 27: 2086–2098. <https://doi.org/10.1101/gad.224899.113>
- [11] XIAO YS, CONG M, LI JT, HE DS, WU QY et al. Cathepsin C promotes breast cancer lung metastasis by modulating neutrophil infiltration and neutrophil extracellular trap formation. *Cancer Cell* 2021; 39: 423–437. <https://doi.org/10.1016/j.ccell.2020.12.012>
- [12] KHAKET TP, SINGH MP, KHAN I, KANG SC. In vitro and in vivo studies on potentiation of curcumin-induced lysosomal-dependent apoptosis upon silencing of cathepsin C in colorectal cancer cells. *Pharmacol Res* 2020; 161: 105156. <https://doi.org/10.1016/j.phrs.2020.105156>
- [13] KHAKET TP, SINGH MP, KHAN I, BHARDWAJ M, KANG SC. Targeting of cathepsin C induces autophagic dysregulation that directs ER stress mediated cellular cytotoxicity in colorectal cancer cells. *Cell Signal* 2018; 46: 92–102. <https://doi.org/10.1016/j.cellsig.2018.02.017>
- [14] SCHREIBER RD, OLD LJ, SMYTH MJ. Cancer Immunoeediting – Integrating Immunity’s Roles in Cancer Suppression and Promotion. *Science* 2011; 331: 1565–1570. <https://doi.org/10.1126/science.1203486>
- [15] ZHUANG XQ, ZHANG H, HU GH. Cancer and Micro-environment Plasticity: Double-Edged Swords in Metastasis. *Trends Pharmacol Sci* 2019; 40: 419–429. <https://doi.org/10.1016/j.tips.2019.04.005>
- [16] JOYCE JA, FEARON DT. T cell exclusion, immune privilege, and the tumor microenvironment. *Science* 2015; 348: 74–80. <https://doi.org/10.1126/science.aaa6204>
- [17] GABRILOVICH DI, ROSENBERG OS, BRONTE V. Coordinated regulation of myeloid cells by tumours. *Nat Rev Immunol* 2012; 12: 253–268. <https://doi.org/10.1038/nri3175>
- [18] DANG YZ, CHEN J, FENG WB, QIAO CY, HAN WL et al. Interleukin 1 β -mediated HOXC10 Overexpression Promotes Hepatocellular Carcinoma Metastasis by Upregulating PDPK1 and VASP. *Theranostics* 2020; 10: 3833–3848. <https://doi.org/10.7150/thno.41712>
- [19] BARVE RA, ZACK MD, WEISS D, SONG RH, BEIDLER D et al. Transcriptional profiling and pathway analysis of CSF-1 and IL-34 effects on human monocyte differentiation. *Cytokine* 2013; 63: 10–17. <https://doi.org/10.1016/j.cyto.2013.04.019>
- [20] MARCHELLI JML, ARDI VC, VIZCARRA EA, ROOIJEN NV, QUIGLEY JP et al. Twist1 Induces CCL2 and Recruits Macrophages to Promote Angiogenesis. *Cancer Res* 2013; 73: 662–671. <https://doi.org/10.1158/0008-5472.CAN-12-0653>
- [21] DOYLE K, LÖNN H, KÄCK H, POËL AVD, SWALLOW S et al. Discovery of Second Generation Reversible Covalent DPP1 Inhibitors Leading to an Oxazepane Amidoacetonitrile Based Clinical Candidate (AZD7986). *J Med Chem* 2016; 59: 9457–9472. <https://doi.org/10.1021/acs.jmedchem.6b01127>
- [22] PALMÉR R, MÄENPÄÄ J, JAUHAINEN A, LARSSON B, MO J et al. Dipeptidyl Peptidase 1 Inhibitor AZD7986 Induces a Sustained, Exposure-Dependent Reduction in Neutrophil Elastase Activity in Healthy Subjects. *Clin Pharmacol Ther* 2018; 104: 1155–1164. <https://doi.org/10.1002/cpt.1053>
- [23] HANAHAHAN D, WEINBERG RA. Hallmarks of cancer: the next generation. *Cell* 2011; 144: 646–674. <https://doi.org/10.1016/j.cell.2011.02.013>
- [24] ABIKO K, MANDAI M, HAMANISHI JZ, YOSHIOKA Y, MATSUMURA N et al. PD-L1 on Tumor Cells Is Induced in Ascites and Promotes Peritoneal Dissemination of Ovarian Cancer through CTL Dysfunction. *Clin Cancer Res* 2013; 19: 1363–1374. <https://doi.org/10.1158/1078-0432.CCR-12-2199>
- [25] SIEMINSKA I, BARAN J. Myeloid-Derived Suppressor Cells in Colorectal Cancer. *Front Immunol* 2020; 11: 1526. <https://doi.org/10.3389/fimmu.2020.01526>

- [26] EYNDE MVD, MLECNIK B, BINDEA G, FREDRIKSEN T, CHURCH SE et al. The Link between the Multiverse of Immune Microenvironments in Metastases and the Survival of Colorectal Cancer Patients. *Cancer Cell* 2018; 34: 1012–1026. <https://doi.org/10.1016/j.ccell.2018.11.003>
- [27] LIAO WT, OVERMAN MJ, BOUTIN AT, SHANG XY, ZHAO D et al. KRAS-IRF2 Axis Drives Immune Suppression and Immune Therapy Resistance in Colorectal Cancer. *Cancer Cell* 2019; 35: 559–572. <https://doi.org/10.1016/j.ccell.2019.02.008>
- [28] ZHU Y, YANG J, XU D, GAO XM, ZHANG Z et al. Disruption of tumour-associated macrophage trafficking by the osteopontin-induced colony-stimulating factor-1 signalling sensitises hepatocellular carcinoma to anti-PD-L1 blockade. *Gut* 2019; 68: 1653–1666. <https://doi.org/10.1136/gutjnl-2019-318419>
- [29] RAZAK AR, CLEARY JM, MORENO V, BOYER M, ALLER EC et al. Safety and efficacy of AMG 820, an anti-colony-stimulating factor 1 receptor antibody, in combination with pembrolizumab in adults with advanced solid tumors. *J Immunother Cancer* 2020; 8: e001006. <https://doi.org/10.1136/jitc-2020-001006>
- [30] OVERMAN MJ, MCDERMOTT R, LEACH JL, SARA LONARDI S, LENZ HJ et al. Nivolumab in patients with metastatic DNA mismatch repair-deficient or microsatellite instability-high colorectal cancer (CheckMate 142): an open-label, multicentre, phase 2 study. *Lancet Oncol* 2017; 18: 1182–1191. [https://doi.org/10.1016/S1470-2045\(17\)30422-9](https://doi.org/10.1016/S1470-2045(17)30422-9)
- [31] CHITTEZHATH M, DHILLON MK, LIM JY, LAOUI D, SHALOVA IN et al. Molecular Profiling Reveals a Tumor-Promoting Phenotype of Monocytes and Macrophages in Human Cancer Progression. *Immunity* 2014; 41: 815–829. <https://doi.org/10.1016/j.immuni.2014.09.014>
- [32] SHI LR, CHEN LJ, WU CQ, ZHU YB, XU B et al. PD-1 Blockade Boosts Radiofrequency Ablation-Elicited Adaptive Immune Responses against Tumor. *Clin Cancer Res* 2016; 22: 1173–1184. <https://doi.org/10.1158/1078-0432.CCR-15-1352>
- [33] PENG DJ, KRYCZEK I, NAGARSHETH N, ZHAO LL, WEI S et al. Epigenetic silencing of TH1-type chemokines shapes tumour immunity and immunotherapy. *Nature* 2015; 527: 249–253. <https://doi.org/10.1038/nature15520>